Unique and complementary information on shape coexistence in the neutron-deficient Pb region derived from Coulomb excitation

Wrzosek-Lipska, K.; Gaffney, L. P.

Published in:
Journal of Physics G: Nuclear and Particle Physics

DOI:
10.1088/0954-3899/43/2/024012

Published: 14/01/2016

Document Version
Peer reviewed version

Unique and complementary information on shape coexistence in the neutron-deficient Pb region derived from Coulomb excitation.

K. Wrzosek-Lipska[1,2]

[1]KU Leuven, Instituut voor Kern- en Stralingsfysica, 3001 Leuven, Belgium
[2]Heavy Ion Laboratory, University of Warsaw, PL-02-093 Warsaw, Poland

E-mail: wrzosek@slcj.uw.edu.pl

L. P. Gaffney[1,3]

[1]KU Leuven, Instituut voor Kern- en Stralingsfysica, 3001 Leuven, Belgium
[3]School of Engineering, University of the West of Scotland, Paisley PA1 2BE, United Kingdom

E-mail: Liam.Gaffney@uws.ac.uk

Abstract. Neutron-deficient isotopes of Pt-Hg-Pb-Po-Rn are the classic region in the investigation of shape coexistence in atomic nuclei. A large programme of Coulomb-excitation experiments has been undertaken at the REX-ISOLDE facility in CERN with a number of even-even isotopes in this region. These experiments have been used to probe the electromagnetic properties of yrast and non-yrast states of even-even exotic nuclei, above and below $Z = 82$. Amongst a large amount of different complementary techniques used to study nuclear structure, Coulomb excitation brings substantial and unique information detailing shape coexistence. In this paper we review the Coulomb-excitation campaign at REX-ISOLDE in the light-lead region together with most recently obtained results. Furthermore, we present some new interpretations that arise from this data and show testing comparisons to state-of-the-art nuclear models.

1. Introduction

Shape coexistence, whereby nuclear states at similar energy exhibit a different deformation appear in the whole nuclear landscape [1], however a classic region for investigating this phenomenon is in the region around $Z = 82$ and the neutron midshell at $N = 104$. The distinctive character of shape coexistence in atomic nuclei lies in the subtle interplay between single-particle and collective behaviour of nucleons. Understanding the delicate balance in between these two opposite trends underpinning structure of atomic nuclei could be a key to reveal the origin of nuclear collectivity and apparent evaporation of the shell structure in atomic nuclei.

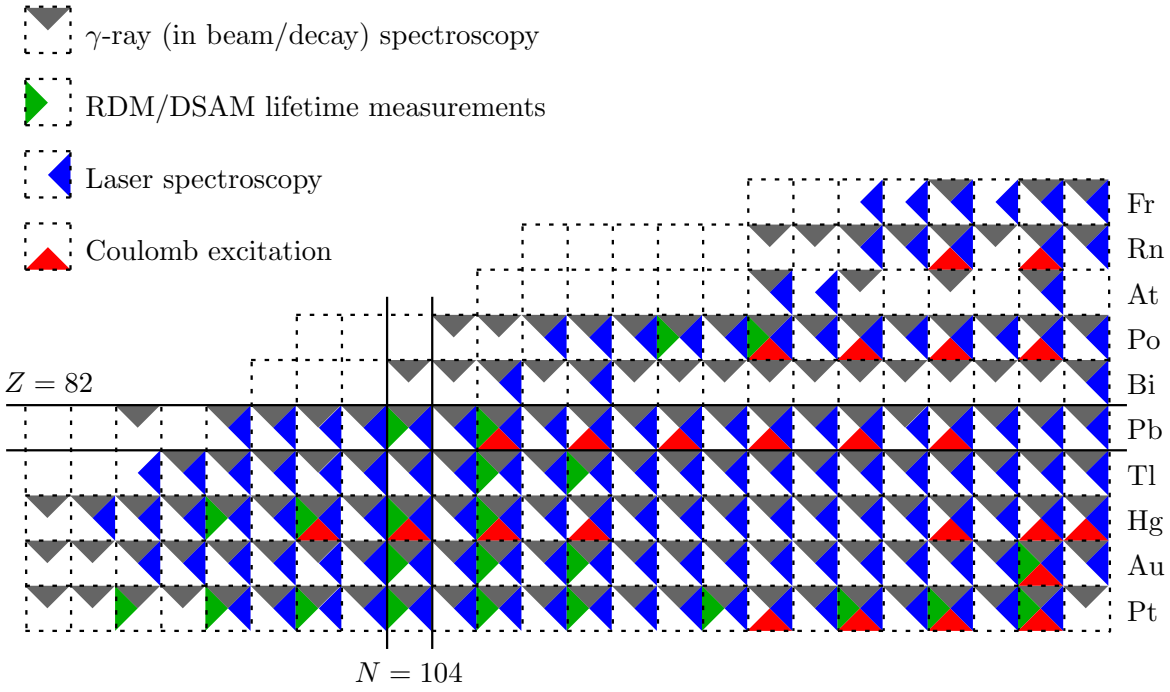

Figure 1. A representation of the nuclear chart in the neutron-deficient Pb region. Isotopes are highlighted by their methods of experimental study appropriate to shape-coexistence studies. Where excited levels have been identified as candidates for rotations built upon the ground-state or as intruder states via γ-ray spectroscopy experiments, that nucleus has been been marked by a downward-pointing grey triangle. Where these levels have been investigated via lifetime measurements a nucleus has been marked by a rightward-pointing green triangle. Nuclei investigated in laser spectroscopy and Coulomb-excitations experiments have been marked with leftward-pointing blue and upward-pointing red triangles, respectively.

Summarised in Fig. 1 is the experimental data collected in the neutron-deficient lead region. A substantial amount of new information has been added or improved upon using various experimental techniques such as: decay studies [2–11], optical spectroscopy studies [12–20], recoil-distance lifetime measurements [21–34] and in-beam γ-ray/electron spectroscopy [35–43]. The contribution to this issue by Julin et. al. [44] details the most recent status of the in-beam experimental studies performed at the Accelerator Laboratory of the University of Jyväskylä, Finland. This wide array of data has provided important indications of shape coexistence in the neutron mid-shell $Z = 82$ region. By example of this, the strong staggering observed in the isotope shifts of the mercury isotopic chain [45, 46] and the early onset of deformation in the light polonium [16] isotopes had particular impact. The structure of $^{186}\mathrm{Pb}_{104}$ inferred from the α-decay measurements of ^{190}Po [3] was interpreted in terms of triple shape coexistence as a competition between three shape minima: oblate, prolate, and the spherical ground state. Global trends of these experimental findings can be reproduced by the theoretical descriptions based on the beyond mean field approaches (see e.g. [47]) or symmetry-guided models (see e.g. [48]). However, more subtle experimental information

on the nature of the quadrupole deformation and on the mixing between the co-existing structures are needed for most of the isotopes in the region. Such data can be provided through the measurements of electromagnetic matrix elements using Coulomb excitation.

Coulomb excitation is a particularly sensitive tool to probe nuclear structure as it selectively excites low-lying states with cross sections being a direct measure of the electromagnetic matrix elements. As the process is governed by the well-known electromagnetic interaction, the nuclear wave functions are probed without the involvement of nuclear forces. Coulomb excitation is thus an excellent experimental method to study nuclear collectivity and deformation of nuclei exhibiting shape coexistence in the Hg-Po-Pb-Rn region.

Low-energy, multi-step Coulomb-excitation experiments can provide unique information on the magnitude and sign of quadrupole moments for a given state. Moreover, while other spectroscopic methods, e.g. lifetime measurements, allow determination of reduced transition probabilities, $B(E2)$ values, the Coulomb-excitation technique brings information on relative signs of transitional matrix elements. Based on the latter, the deformation parameters of the charge distribution in the intrinsic frame of the nucleus can be determined in a nuclear-model independent manner using the rotational-invariant method [49, 50] (see Sec. 3.1).

With recent advances in ISOL-based radioactive ion beam (RIB) facilities [51], low-energy Coulomb excitation became a very well suited technique to study the electromagnetic properties of unstable nuclei. A broad review on low-energy Coulomb-excitation studies of exotic nuclei is given in Ref. [52]. The main challenge of the experiments performed with RIBs is the beam intensity, nowadays typically of order the of 10^4–10^5 pps. When Coulomb excitation is used in the context of exotic beams often a single-step excitation of the first-excited 2_1^+ state in even-even nuclei is observed. Nevertheless, in some cases (e.g. [53–55]), the use of high-Z projectiles yields multi-step excitation, involving more low-lying yrast and non-yrast states. Such experiments lead to the extraction of electromagnetic matrix elements between populated states, however a comprehensive picture of the underlying physics can only be obtained involving a complementary set of experimental data, as shown in Fig. 1. The uniqueness of Coulomb excitation technique lies in providing an access to subtle, higher-order effects, such as spectroscopic quadrupole moments of excited states and signs of interference terms (relative signs of transitional matrix elements). However to determine the latter a complementary information from the independent measurements of lifetimes, γ-ray branching ratios and mixing coefficients is often needed to be used providing important constraints. Results obtained from such combined analysis, merging different sets of data, enable to understand the origin and nature of shape coexistence phenomena in atomic nuclei.

2. Experiments and Results

2.1. REX-ISOLDE Facility

A campaign of Coulomb-excitation experiments in the neutron-deficient Pb region have taken place in recent years at the REX-ISOLDE facility, CERN [53, 56–59]. REX-ISOLDE is unique worldwide in being able to produce and post-accelerate such beams of heavy nuclei with the purity required for precision Coulomb-excitation measurements. To achieve this, an array of state-of-the-art ion-sources are available for the extraction of a large range of isotopes from thick uranium carbide or molten lead primary targets, following their production driven by 1.4 GeV protons from CERN's Proton Synchrotron Booster. For the polonium (see Sec. 2.4) and lead (see Sec. 2.3) Coulomb-excitation experiments, the RILIS ion-source [60] was employed to selectively ionise the element of interest. In the case of mercury (see Sec. 2.2) and radon (see Sec. 2.5), the VADIS ion-source [61] was used; in the latter of these, a cooled transfer line was employed in order to suppress contamination from more volatile elements.

After extraction as singly-charged positive ions from the ion source, the beam undergoes mass separation in either the High-Resolution (HRS) or General-Purpose Separators (GPS) and are fed into the ion trap, REX-TRAP [62], for bunching. The charge state of the ions is then bred in the electron beam ion source, REX-EBIS [63], to achieve a suitable mass-to-charge ratio of $A/q < 4.5$ for injection to the linear post-accelerator, REX-LINAC [64]. The final energy of the beams in this campaign was between 2.8 and 2.9 MeV/u. The post-accelerated radioactive ion beams were then Coulomb excited on secondary targets inside of the Miniball Ge-detector array [65] with recoils and projectiles detected in forward laboratory angles in a double-sided silicon strip detector (DSSSD) as depicted in Fig. 2. Target species and thicknesses used were selected depending on the investigated isotope. Considerations to be made in this choice include the kinematics of the reaction and the cross-section of scattering and excitation of the projectile. Furthermore, one must consider the cross-section of target excitation since de-excitation γ rays from the target will also be present in the spectra. A careful choice is required in order to have no overlapping transitions and yet still have sufficient target excitation to provide, if necessary, a good normalisation of the projectile cross-sections [66]. If lifetimes of excited states are known in the projectile, this provides an internal normalisation and low target cross-sections are desirable. Table 1 summarises all of the experimental details of the campaign.

2.2. Mercury isotopes ($Z = 80$)

Low-energy nuclear states of exotic nuclei from the neutron-deficient lead region were populated in the Coulomb excitation experiments. The de-exciting γ-rays were measured in the coincidence with scattered recoils and projectiles. As an example the γ-ray energy spectrum collected for ^{184}Hg is presented in Figure 4. Clearly, γ-ray peaks associated with the depopulation of the 2_1^+, 4_1^+ and 2_2^+ states are visible. Similar

Table 1. Summary of Coulomb-excitation experiments in the Hg-Rn region carried out at REX-ISOLDE.

Isotope	Primary target	Ion source	Charge state	Energy (MeV/u)	Intensity (ions/s)	Secondary target	Year	Ref.
^{182}Hg	Pb	VADIS	44^+	2.85	3.5×10^3	^{112}Cd	2008	[53, 54]
^{184}Hg	Pb	VADIS	43^+	2.85	4.8×10^3	^{120}Sn	2007	[53, 54]
						^{107}Ag	2007	[53, 54]
			44^+		2.2×10^4	^{112}Cd	2008	[53, 54]
^{186}Hg	Pb	VADIS	43^+	2.85	2.1×10^5	^{120}Sn	2007	[53, 54]
						^{107}Ag	2007	[53, 54]
			44^+		3.0×10^4	^{114}Cd	2008	[53, 54]
^{188}Hg	Pb	VADIS	44^+	2.85	1.6×10^5	^{120}Sn	2007	[53, 54]
						^{107}Ag	2007	[53, 54]
			45^+		1.0×10^5	^{114}Cd	2008	[53, 54]
^{188}Pb	UC_x	RILIS	45^+	2.82	3.2×10^5	^{112}Cd	2011	[56]
^{190}Pb	UC_x	RILIS	45^+	2.82	2.2×10^5	^{112}Cd	2011	[56]
^{192}Pb	UC_x	RILIS	45^+	2.84	5.0×10^5	^{112}Cd	2010	[56]
^{194}Pb	UC_x	RILIS	45^+	2.82	7.8×10^5	^{112}Cd	2011	[56]
^{196}Pb	UC_x	RILIS	45^+	2.82	5.0×10^5	^{112}Cd	2011	[56]
^{198}Pb	UC_x	RILIS	45^+	2.82	2.5×10^5	^{112}Cd	2011	[56]
^{196}Po	UC_x	RILIS	48^+	2.85	2.3×10^4	^{104}Pd	2012	[57, 67]
^{198}Po	UC_x	RILIS	48^+	2.85	4.6×10^4	^{94}Mo	2012	[57, 67]
^{200}Po	UC_x	RILIS	48^+	2.85	2.5×10^5	^{104}Pd	2009	[57, 67]
^{202}Po	UC_x	RILIS	49^+	2.86	6.6×10^4	^{104}Pd	2012	[57, 67]
					4.6×10^4	^{94}Mo	2012	[57, 67]
^{206}Po	UC_x	RILIS	49^+	2.85	–†	^{104}Pd	2012	[59]
^{202}Rn	UC_x	VADIS	47^+	2.90	2×10^4	^{109}Ag	2008	[58]
				2.845	4×10^4	^{120}Sn	2010	[58]
				2.28	3×10^3	^{109}Ag	2008	[58]
^{204}Rn	UC_x	VADIS	47^+	2.90	2×10^5	^{109}Ag	2008	[58]
						^{120}Sn	2008	[58]
				2.28	4×10^4	^{109}Ag	2008	[58]
^{208}Rn	UC_x	VADIS	50^+	2.82	5.6×10^5	^{116}Cd	2010	[59]
^{210}Rn	UC_x	VADIS	51^+	2.82	2.1×10^5	^{116}Cd	2010	[59]

† ^{206}Po was extracted "offline" from the UC_x target in the absence of the primary proton beam. Therefore, the beam intensity was not constant over time and is not defined.

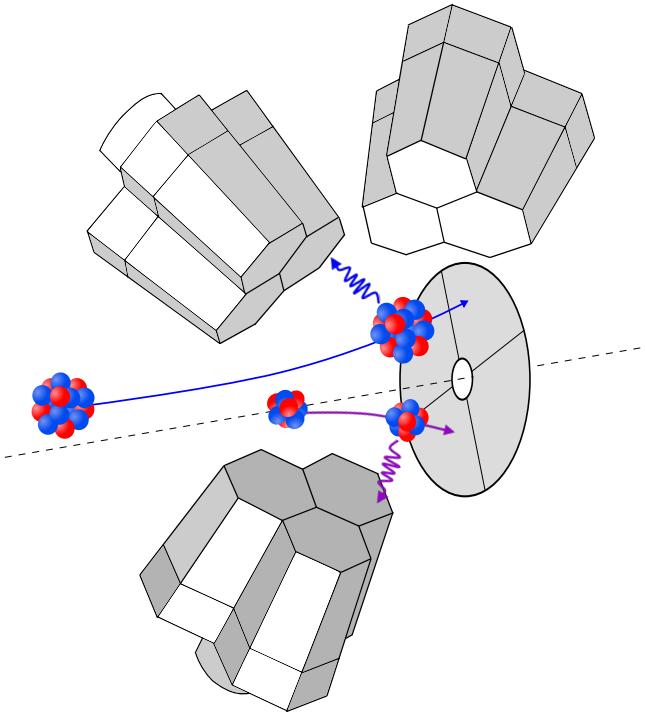

Figure 2. A schematic representation of the Coulomb-excitation experiments performed with Miniball at REX-ISOLDE in this campaign. A heavy radioactive ion is impinged on lighter target species and both the scattered projectile and recoiling target nucleus are forward focused in the laboratory frame of reference. This allows coincident detection of both scattering partners in the DSSSD detector of Miniball, along with the deexcitation γ-rays that follow inelastic events.

spectra were collected for ^{182,186,188}Hg and the states populated in all cases are shown in Fig. 3. Additionally, a weak population of the 4_2^+ state in ^{184,186}Hg and 2_3^+ state in ^{184}Hg was observed. Moreover, an intense K-shell X-ray peaks are observed in the spectra. A detailed analysis of these peaks, that were Doppler-broadened, revealed that they originate partly from the heavy-ion induced K-vacancy creation process when the mercury beam passes the target [54, 68] and partly from known electron conversion accompanying the observed transitions in mercury. Taking both these effects into account still a significant amount of X rays remained, which were attributed to $E0$ deexcitation. From their intensities the population of the 0_2^+ and 2_2^+ states, decaying via strongly converted transitions to the ground 0_1^+ and 2_1^+ states, respectively, was deduced [54, 69].

These experiments showed the possibility of populating non-yrast states, whose

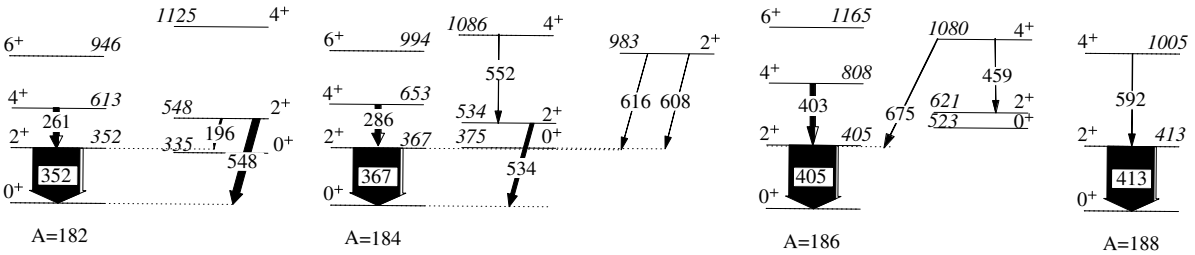

Figure 3. Part of the low-energy level schemes of the even-even $^{182-188}$Hg isotopes. Widths of the arrows are proportional to the observed γ-ray intensities normalised to the $2_1^+ \rightarrow 0_1^+$ transition. Energies of γ-ray transitions and levels (italics) are given in keV. Adapted from Ref. [53].

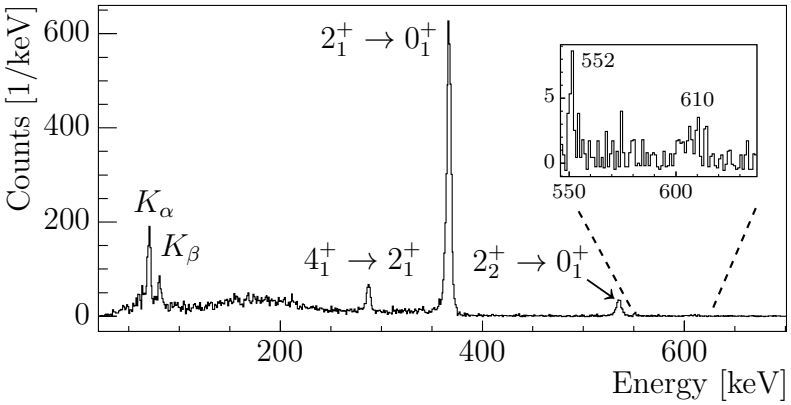

Figure 4. γ-ray energy spectrum following the Coulomb excitation of ^{184}Hg induced by a ^{120}Sn target, Doppler-corrected for transitions in ^{184}Hg. The population of the yrast and non-yrast states in ^{184}Hg as well as intense mercury K-shell X ray peaks are observed. The inset shows part of the spectrum where a weak $4_2^+ \rightarrow 2_2^+$ γ-ray peak (552 keV) and ($2_3^+ \rightarrow 0_2^+$ and $2_3^+ \rightarrow 2_1^+$) doublet (around 610 keV) in ^{184}Hg are visible.

electromagnetic properties are crucial to understand shape coexistence in nuclei in the $N \approx 104$ mid-shell region. The GOSIA [70, 71] code was used for the analysis of Coulomb-excitation data and the methods used in all of the cases discussed here have recently been detailed in Ref. [66]. These data were combined with the additional spectroscopic information known for mercury isotopes in the final analysis – independently measured lifetimes [30, 34], γ-ray branching ratios and electron conversion coefficients – and a set of matrix elements, involving all states populated in even-even $^{182-188}$Hg, has been obtained. The quadrupole deformation for the ground and intruder 0^+ states was concluded for the first time and is described in more details in Section 3.1.

Primary production yields of the most neutron-deficient mercury isotopes begin to limit the possibility of extending these measurements further. Advances, such as the molten Pb target and an increased primary proton beam energy may open the possibility in the future.

2.3. Lead isotopes ($Z = 82$)

Yrast 2^+ states were populated in all investigated Pb nuclei (listed in Table 1), while the non-yrast 2^+ states were additionally observed in ^{188,192}Pb. As in the mercury case, an excess of K-shell X rays was extracted from the data. One of the challenges when performing Coulomb excitation experiments at REX-ISOLDE can be isobaric impurity in the beam, which was an important issue for measurements performed with Pb (and Po) isotopes. In the raw γ-ray energy spectra of the Pb Coulomb-excitation experiments [56] an isobaric contamination from the Tl isotopes is clearly visible. While the Pb isotopes are selectively ionised with RILIS, the highly-reactive Tl is ionised by the hot metal surface along the transfer line between the target and ion source. This process can be treated as independent from the laser ionisation and therefore, by switching the laser ionisation on and off, the Pb events can be revealed. To do this, the

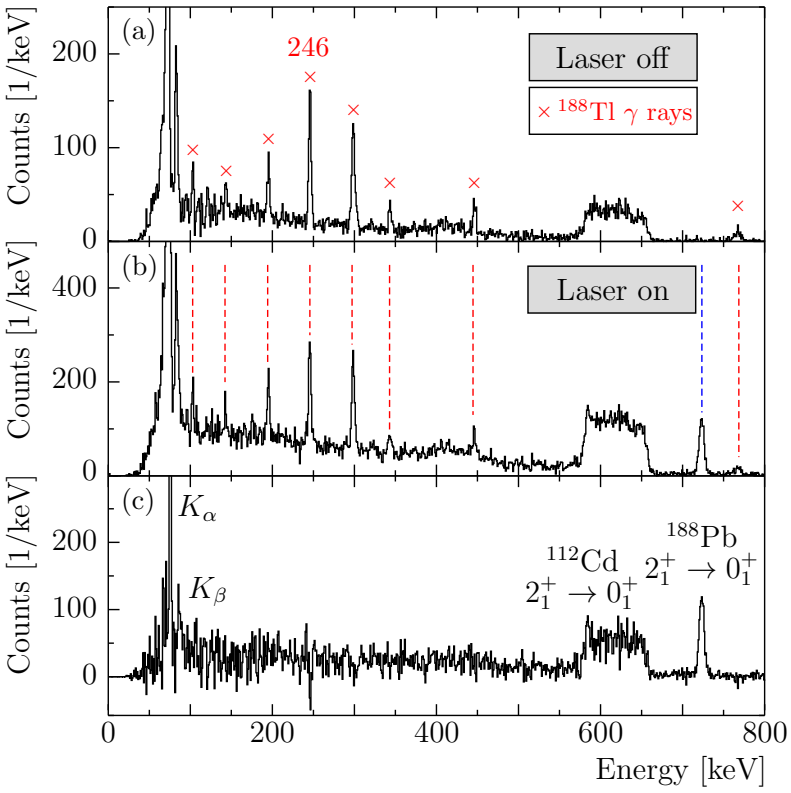

Figure 5. γ-ray energy spectra following the Coulomb excitation of ^{188}Pb and the ^{188}Tl contaminant induced by a ^{112}Cd target, Doppler-corrected for transitions in the projectile. (a) "Laser on" data collected while the ionising laser was not incident in the ion source. (b) "Laser off" data collected with the ionising laser on and illuminating the ion source. (c) "Laser on" data with the normalised "Laser off" data subtracted. The population of the first-excited 2^+ state in ^{188}Pb is visible (dashed blue line) along with an excess of K-shell X ray peaks and all other peaks associated with the contaminants (dashed red lines) have been subtracted. The excitation of the recoiling ^{112}Cd nuclei is also observed as a Doppler "smeared" bump around 620 keV. Adapted from Ref. [56].

data sets of laser on/off are normalised and subtracted to leave a pure Pb data set as illustrated in Fig. 5. The resulting γ-ray energy spectra are free of Tl contamination and the corresponding target excitation can be attributed to Pb without need for further correction. The contamination for lighter masses begins to dominate over the more and more weakly produced isotope of interest, limiting the reach of Coulomb excitation to $A \gtrsim 186$. This famous case of ^{186}Pb [3], with its first two excited states having $J^+ = 0^+$, is the perfect target nucleus for the new SPEDE electron detector to be mounted in the Miniball array [72]. Developments are on-going to achieve the required purity at $A = 186$ at HIE-ISOLDE, while a proposal is already accepted for renewed Coulomb excitation of ^{188}Pb at higher energies and with SPEDE in place [73].

2.4. Polonium isotopes ($Z = 84$)

Going further, towards higher proton number $Z = 84$, the neutron-deficient ^{196,198,200,202,206}Po isotopes were studied utilising the Coulomb-excitation technique. For the cases of ^{200,202}Po the 2_1^+ state was exclusively populated. For such cases the Coulomb-excitation cross-section calculation is affected by three parameters, namely $\langle 0_1^+ \| E2 \| 2_1^+ \rangle$, $\langle 2_1^+ \| E2 \| 2_1^+ \rangle$ and the absolute normalisation. The normalisation is fitted to the target excitation, deduced from its de-excitation γ-ray intensity. By utilising the granularity of the Miniball DSSSD detector [65], sensitivity to the second-order effect, such as the diagonal matrix element $\langle 2_1^+ \| E2 \| 2_1^+ \rangle$, can be reached. In the ^{200}Po experiments, the number of data allowed a segmentation into fourteen different scattering angles, enabling a differential analysis of the 2_1^+ excitation cross-section. This leads to a determination of the diagonal matrix element, $\langle 2_1^+ \| E2 \| 2_1^+ \rangle$, or equivalently the spectroscopic quadrupole moment, Q_s, to a precision of 0.2 eb in ^{200}Po [57, 67].

Moreover, as in the case of mercury isotopes, multistep Coulomb excitation was observed in ^{196,198}Po yielding 4_1^+, 2_2^+ and 0_2^+ state population. The latter was deduced from the intensity of observed K-shell X rays, analogously as it was done for the mercury isotopes [67]. Just like the lead isotopes, the more neutron-deficient polonium isotopes begin to be dominated by contamination meaning that these experiments pushed the current limit of precision measurements. In ^{196}Po, the beam purity was $\approx 60\%$ after the substantial enhancement of the laser ion source, RILIS.

2.5. Radon isotopes ($Z = 86$)

Two very neutron-deficient radon isotopes were studied, ^{202,204}Rn [58] as well as two heavier-mass isotopes ^{208,210}Rn. On the lighter side, shape coexistence can be expected as in the case of the "mirror" isotopes about $Z = 82$, platinum. While the low-lying structure of ^{202}Rn could be interpreted as vibrational-like or a gamma-soft rotor, critical states are so far unobserved, such as the 0_2^+ state. In the shape-coexistence picture, an excited 0^+ state is key to characterising the intruder structure and its decay behaviour is the perfect test of the vibrational description. For this reason, the Coulomb-excitation study of ^{202,204}Rn proceeded in two parts. Firstly, a ^{109}Ag target was used to provide a good normalisation for measurement of the $B(E2; 2_1^+ \rightarrow 0_1^+)$ values. Secondly, a ^{120}Sn target, with its higher Z value and low excitation cross-section, allowed for a clean observation of higher-lying states populated in two-step processes. As can be seen in the spectrum of Fig. 6, the 2_2^+ and 4_1^+ states were observed in ^{202}Rn, but unfortunately no evidence was found for a new 0_2^+ state, which remains elusive. However, the measurement of a larger than expected $B(E2; 2_2^+ \rightarrow 2_1^+)$ casts strong doubt on the vibration argument. A gamma-soft description can not be ruled out and more precise $B(E2)$ values would be a good test of this. In the ^{204}Rn experiments, no higher-order excitations were observed in the ^{120}Sn data set. Many experiments with RIBs are now benefiting from changing the target species (Z). This provides a further disambiguation between different multi-step excitation pathways, which turns out to be important. With

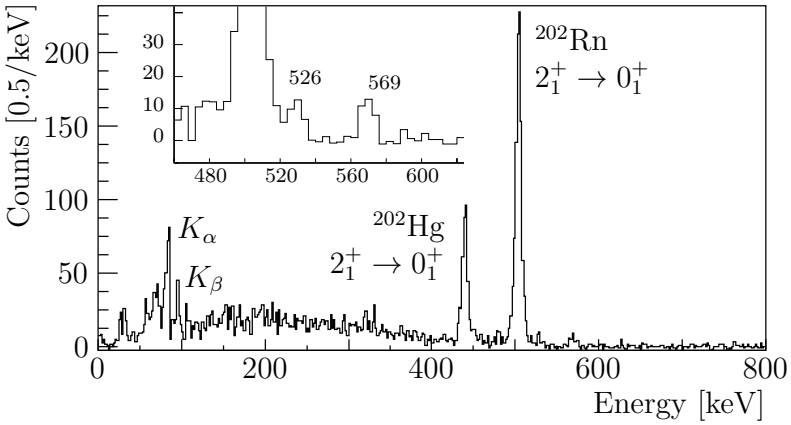

Figure 6. γ-ray energy spectrum following the Coulomb excitation of ^{202}Rn induced by a ^{120}Sn target, Doppler-corrected for transitions in ^{202}Rn. The first-excited 2^+ state in ^{202}Rn is populated and, more weakly, the 2_2^+ and 4_1^+ states (inset shows the 526-keV $2_2^+ \rightarrow 2_1^+$ and 569-keV $4_1^+ \rightarrow 2_1^+$ transitions with a 4 keV bin width). Additionally, an excess of K-shell X rays is observed, just as in the Hg, Pb and Po cases. Isobaric contamination was present in the beam from the stable ^{202}Hg, which is also excited and can be observed in the γ-ray spectrum. Adapted from Ref. [58].

the limited geometry that is dictated by the inverse kinematics reactions, the scattering angle sensitivity alone cannot always provide the sensitivity required.

Future measurements should focus on identification and characterisation of excited 0^+ states in the lightest radon isotopes. A range of techniques could achieve this, including α-decay measurements and in-beam conversion-electron spectroscopy. Coulomb excitation at higher energies in the nuclei already studied would give a vast amount of new information on higher-lying states that can test model predictions, which so far remains imprecise.

3. Interpretation

A set of matrix elements obtained in Coulomb-excitation experiments can be analysed in terms of quadrupole deformation. The approach used is the rotational-invariant method, relating the reduced $E2$ matrix elements with deformation parameters. It conveniently allows the merger of a large set of experimental results into a compact form, giving insight into the charge distribution of a nucleus in a given state. Details are described in Sect. 3.1. On the other hand, $E2$ matrix elements can be interpreted within a simple, phenomenological two-state mixing model. An assumption that the structure of neutron-deficient mercury or polonium isotopes can be described by two distinct configurations which mix at low excitation energies can be tested. This issue is addressed in Sec. 3.3. Finally, as the electromagnetic matrix elements are a sensitive probe of nuclear states and their wave functions, these results serve as a stringent test of the most modern and frequently used state-of-art models based on beyond mean-field and interacting boson approaches. A compact overview is given in Sec. 3.4.

3.1. Quadrupole deformation inferred from the rotational-invariant method

The only observables related to the quadrupole collectivity and shape of a nucleus are the reduced transition probabilities, $B(E2)$ values, and spectroscopic quadrupole moments. Coulomb excitation provides essential information on diagonal and non-diagonal matrix elements, including their relative signs, based on which various moments describing nuclear deformation can be extracted in a nuclear model-independent way. This was presented by Kumar, Cline and others [49, 50, 55, 74, 75] and is known as the quadrupole sum rules method. It is based on the fact that the electric multipole transition operator, $E(\lambda, \mu)$, is a spherical tensor and thus its zero-coupled products can be formed, which are rotationally invariant.

The lowest-order products of $E2$ operator provide information on the intrinsic quadrupole deformation parameters of a nucleus – the overall quadrupole deformation (Q^2) and nonaxiality parameter ($\cos(3\delta)$). These invariants can be related to the general Bohr Hamiltonian [76] collective shape variables β and γ, respectively, as shown in [75].

In the laboratory frame the expectation values of these two basic quadrupole invariants can be expressed by the set of $E2$ matrix elements as given by the following two equations:

$$\begin{aligned}\frac{\langle Q^2\rangle}{\sqrt{5}} &= \langle i \,\|[E2\times E2]_0\|\, i\rangle \\ &= \frac{(-1)^{2I_i}}{\sqrt{(2I_i+1)}}\cdot\sum_t \langle i\|E2\|t\rangle\langle t\|E2\|i\rangle \begin{Bmatrix} 2 & 2 & 0 \\ I_i & I_i & I_t \end{Bmatrix},\end{aligned} \tag{1}$$

and

$$\begin{aligned}\sqrt{\frac{2}{35}}\langle Q^3\cos(3\delta)\rangle &= \langle i \,\big\|[[E2\times E2]_2\times E2]_0\big\|\, i\rangle \;= \\ &= \frac{(\pm 1)}{(2I_i+1)}\cdot\sum_{t,u}\langle i\|\mathrm{E2}\|u\rangle\langle u\|\mathrm{E2}\|t\rangle\langle t\|\mathrm{E2}\|i\rangle \begin{Bmatrix} 2 & 2 & 2 \\ I_i & I_t & I_u \end{Bmatrix},\end{aligned} \tag{2}$$

where a negative sign corresponds to the integer spin system, while a positive one to the half-integer spin system. The sums in Eqs. 1 and 2, which extend over all intermediate states, are in practice limited to the few most significant $E2$ matrix elements (see e.g. [49]), which depends on the degree to which nuclear properties are correlated by collective degrees of freedom. In the example of ^{100}Mo [75] it was shown that the contributions from the first three 2^+ states very well describe the Q^2 invariant and in 97% approximate calculated expectation values of $Q^3\cos(3\delta)$. What is worth noting is the fact that to get information on triaxiality more subtle experimental data are required – not only transitional $E2$ matrix elements are important, but also their relative signs and quadrupole moments. This is shown schematically in Fig. 7 for the case of the 0^+ ground state. In general, the quadruple sum rules method can be applied to any excited state only if a large enough set of matrix elements is known coupling a given state of interest with all others populated through a single-step $E2$ transition.

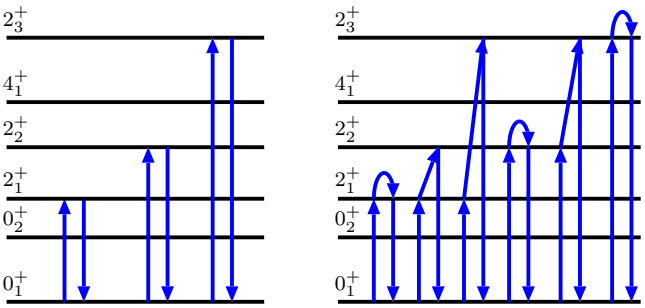

Figure 7. A schematic illustration of an example products of $E2$ matrix elements taken into account to calculate lowest order invariants: $\langle Q^2 \rangle$ (*left*) and $\langle Q^3 \cos(3\delta) \rangle$ (*right*) for the case of the 0^+ ground state of even-even nucleus.

The quadrupole sum rules method is particularly useful to attribute shape parameters to low-lying 0^+ states, which deformation cannot be directly inferred from e.g. quadrupole moment measurement. The afore-mentioned method was applied to analyse the character of deformation for low-lying 0^+ states in even-even, neutron-deficient $^{182-188}$Hg isotopes [53]. It was shown (see Fig. 8) that the ground states of the $^{182-188}$Hg isotopes are weakly deformed and of predominantly oblate-like character, while the excited 0^+ states appear to be clearly more deformed. The lack of accuracy on some key matrix elements prevents drawing firm conclusions on the nature of the deformation of the excited 0^+ state, however triaxiality seems to be not excluded in ^{182,184}Hg.

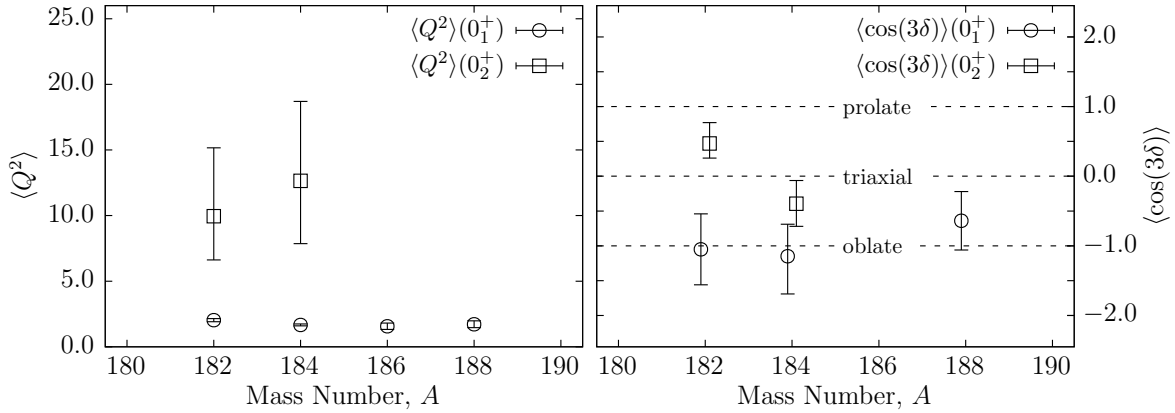

Figure 8. The $\langle Q^2 \rangle$ and $\langle \cos(3\delta) \rangle$ values representing the overall deformation and the axial asymmetry, respectively of the 0_1^+ (open squares) and 0_2^+ (full squares) states in $^{182-188}$Hg. These were extracted from the matrix elements obtained in [53].

3.2. Comparison to charge radii

Changes in mean-square-charge radii along an isotopic chain can shed light upon the development of deformation in the ground state by using comparisons to the modified liquid-drop model [14, 77]:

$$\langle r^2 \rangle_A \approx \langle r^2 \rangle_A^{\mathrm{sph}} \left(1 + \frac{5}{4\pi} \langle \widetilde{\beta}_2^2 \rangle_A \right) , \tag{3}$$

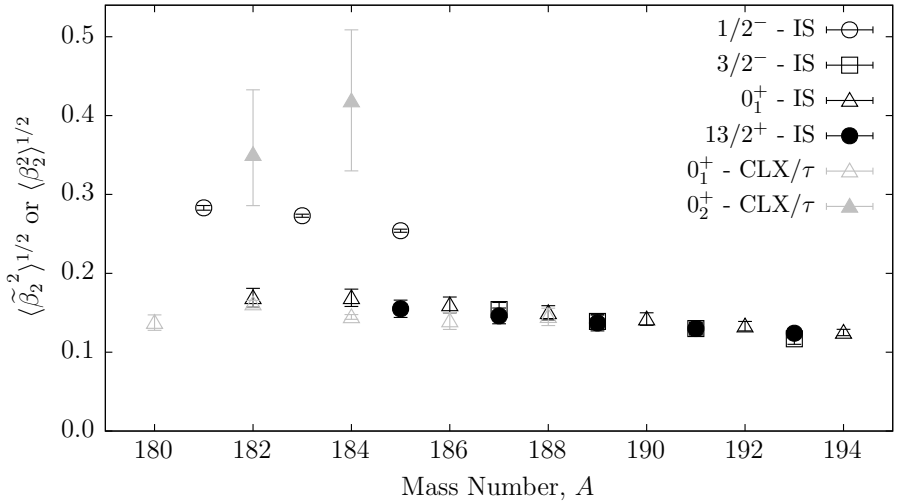

Figure 9. Quadrupole deformation parameters deduced from isotope shift (IS), lifetime (τ) and Coulomb-excitation (CLX) data for ground and isomeric states and additionally, excited 0^+ states in ^{182,184}Hg. Isotope shift data are taken from Refs. [46] and $\langle\widetilde{\beta_2^2}\rangle^{1/2}$ is calculated following the method of Ref. [14]. New data will soon be available from RILIS-ISOLDE [20]. Values extracted from $B(E2)$ values in Coulomb-excitation and lifetime measurements, $\langle\beta_2^2\rangle^{1/2}$, are determined by Eq. 1 of Ref. [58] and their uncertainties are calculated including correlations from the Coulomb-excitation analysis, where available.

where $\langle r^2\rangle_A^{\rm sph}$ is the mean-square charge radius of a spherical liquid-drop-like nucleus with mass, A. One of the major tools involved in beam production at ISOLDE is the Resonant Ionisation Laser Ion Source (RILIS). Not only does it provide a large fraction of the ion source requirements for users, it is also used as a powerful spectroscopic device to measure isotope shifts and consequently, differences in mean-square-charge radii. A comprehensive review of the in-source laser spectroscopy program at RILIS-ISOLDE was recently undertaken by Marsh et al. [60]. Importantly, long isotopic chains of Hg [20], Pb [13] and Po [14, 16] have been measured. Furthermore, a previous collinear setup at ISOLDE yielded isotope shift and hyperfine measurements in Rn [78, 79].

Often the sensitive technique of laser spectroscopy can reach further from the valley of stability than methods such as recoil distance lifetime measurements and Coulomb excitation. Therefore, it is worthwhile to be able to compare the results of these complementary approaches to determining ground-state deformation to garner confidence in the respective techniques. Fig. 9 shows such a comparison for the Hg isotopic chain. Recent data from the *In-source laser spectroscopy of mercury isotopes* experiment at RILIS-ISOLDE [20] is under analysis and will extend the deformation systematics down to ^{177}Hg. Not only the trend but also the magnitude of extracted deformation parameter shows very good consistency between the two methods. Similar conclusions are also drawn for the Po [57] and Rn [58] isotopic chains where data are available.

The now famous case of large odd-even staggering in the Hg isotopes around

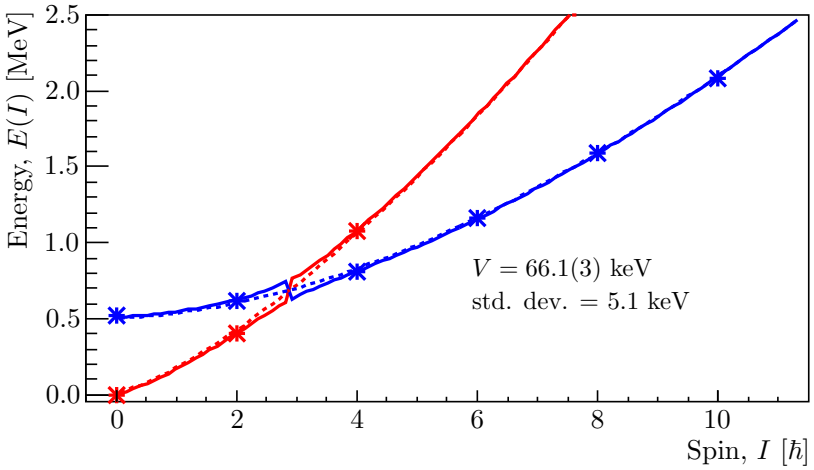

Figure 10. Variable Moment of Inertia (VMI) fits of the normal (red) and intruder (blue) bands in ^{186}Hg, performed in Ref. [34]. The dashed lines show the pure behaviour of the bands, while the solid lines include a spin independent mixing parameter, V, to which the experimentally observed levels (crosses) are fitted. Here, a priori assignments of the experimental levels to each band is required and various assumptions were tested. The crossing of the bands can be seen around $I = 3$, indicating that the 4^+_1 state is predominantly of the intruder configuration.

$^{181-185}$Hg [46] has long been attributed to the intruder structure becoming the ground state in the odd-mass isotopes. One might expect that the deformation of the excited 0^+_2 state in the neighbouring even-mass isotopes, also attributed to the intruder structure, is comparable to that of the odd-mass ground states. While both have enhanced deformations, there exists a deviation between the values such that the 0^+_2 state in ^{182,184}Hg has a larger deformation than the $1/2^-_1$ state in ^{181,183,185}Hg. Firm conclusions cannot yet be drawn, however, due to the lack of precision in the determination of the 0^+_2-state deformation from the Coulomb-excitation measurements.

3.3. Two-state mixing model

The phenomenological Variable Moment of Inertia (VMI) model [80] has been successful in describing the ground-state rotational bands of many even-even nuclei by introducing a certain degree of "softness" as a second parameter. This description has been extended to cases with intruding bands by introducing a spin-independent mixing matrix element. In the case of the mercury isotopes, where oblate- and prolate-like bands coexist, the VMI mixing approach has been taken [34] with considerable success. An example of the fit in ^{186}Hg is shown in Fig. 10. From this, the mixing amplitudes of each state can be extracted following the formalism of Ref. [81]. While these results alone can tell a story, a quantitive comparison of the resultant $B(E2)$ values proves a much more powerful indicator of the two-band picture [34]. Indeed, more powerful still is the possibility of comparing matrix elements, including their signs, extracted from Coulomb excitation measurements [53]. For all four mercury isotopes studied, a common set of "pure"

matrix elements was assumed for the normal (n) and intruder (i) bands, consisting of $\langle 0^+_{n,i} \| E2 \| 2^+_{n,i} \rangle$ and $\langle 2^+_{n,i} \| E2 \| 2^+_{n,i} \rangle$, while the "pure" inter-band matrix elements are assumed to vanish. Using only these four matrix elements as free parameters and invoking the mixing amplitudes extracted from the VMI mixing fits [34], a remarkable reproduction of the experimental values is found. Only for a few matrix elements is a significant deviation ($> 3\sigma$) observed, and in most of these cases only the sign differs, not the magnitude. The fit yields "pure" matrix element values consistent with a weakly deformed oblate coexisting with a more strongly deformed prolate structure [53].

A similar exercise was performed in the polonium isotopes and is detailed in Refs. [57, 67]. While the intruder band can be well described by the VMI description, the normal, weakly-deformed structure cannot. A different approach was taken to extract the mixing amplitudes in this case with the assumption of a constant mixing matrix element ($V = 200$ keV) across all studied isotopes. These resulting "pure" matrix elements values describe the ground state normal structure as almost spherical [57, 67]. What is interesting to note though is the similarity between the "pure" matrix elements of the intruder structure in polonium and the "pure" matrix elements in the normal structure of mercury [53], implying a similar shape of these two structures.

3.4. Comparison to state-of-the-art models

Electromagnetic matrix elements are a sensitive probe of nuclear wave functions so that Coulomb-excitation measurements, combined with in-beam and decay studies, provide an extremely stringent test of state-of-art nuclear models. The experimental results obtained for neutron-deficient mercury [53, 54], polonium [57] and radon [58] isotopes were compared with several theoretical approaches: the beyond mean-field model (BMF) [47], the generalised Bohr Hamiltonian model (GBH) [76] and the interacting boson model with configuration mixing (IBM-CM) [48]. The first two approaches are based on the self-consistent mean-field calculations using the Hartree-Fock-Bogoliubov (HFB) method and the Skyrme SLy4 interaction.

The collective quadrupole general Bohr Hamiltonian is determined by seven functions (seven inertial functions and potential energy) which are derived from the microscopic theory using the adiabatic time-dependent Hartree-Fock-Bogoliubov (ATDHFB) approach. In this method no additional free parameters are introduced and the prediction of collective properties is based solely on the knowledge of effective nucleon-nucleon interactions. However, the cranking approximation of the ATDHFB used in the calculations neglects the effects of a time-odd component of the mean field induced by a collective motion. Due to technical difficulties in most applications, including present work,such effects are taken into account simply by rescaling the derived inertial functions by a constant factor being typically in the range of 1.2 –1.4 [75, 76].

One of the advantages of the GBH is that it permits treatment of all quadrupole degrees of freedom, including non-axiality and rotations, on equal footing. The GBH approach differs in this respect from the one used by Yao et al. [47] in the BMF model

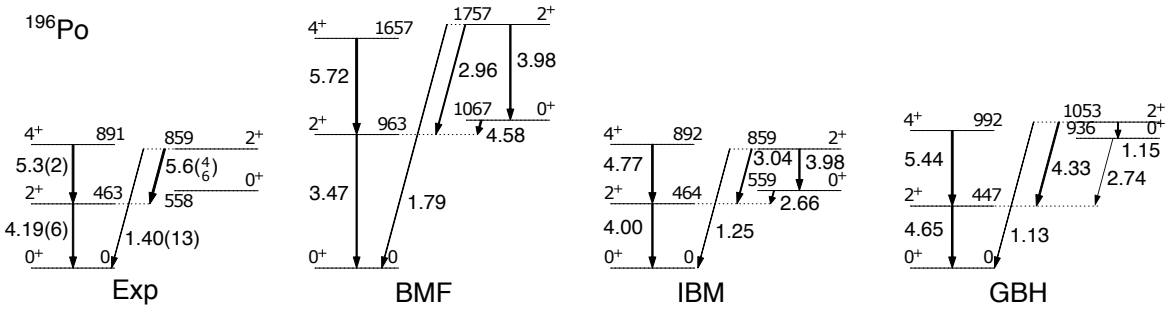

Figure 11. Experimental level scheme and Q_t values in ^{196}Po compared to the predictions of calculations performed within the Beyond-Mean-Field (BMF) [47], Interaction-Boson (IBM) and General-Bohr-Hamiltonian (GBH) models. Adapted from Ref. [57].

where the axially symmetric mean-field wave functions are first projected on angular momentum and particle number, and then mixed with respect to the axial quadrupole moment. As stated in Ref. [47], the currently available computational resources prevent systematic calculations including triaxial degrees of freedom to be performed for very heavy nuclei. This can be one of the reasons for the systematic over expansion of excitation spectra obtained from the BMF calculations in the Hg-Po-Rn region, as discussed further in this section. In both the BMF model and GBH approaches the only parameters are those of the energy density functional and no specific adjustments are performed in their applications to the neutron-deficient isotopes around lead. There is a contribution to this issue by Heenen et. al. [82] detailing the BMF approach specific to shape coexistence. In the case of the IBM-CM model the parameters of the Hamiltonian are fitted to a number of experimental data and adjusted for each isotope of interest. Therefore its ability to make predictions is rather limited and it is more suited to study the importance of configuration mixing and its impact on understanding the nuclear structure. Characteristic features of the mean-field approaches, in contrast to the IBM model, is the use of quantities directly related with the nuclear mass distribution, in other words, the shape of the nucleus.

Figure 11 shows a comparison of the experimentally observed partial level schemes and transition probabilities, expressed in terms of transition quadrupole moments $|Q_t|$, and the predictions of the afore-mentioned nuclear models, using ^{198}Po as an example. It can be noted that the BMF calculation overestimates the absolute values of the energy levels, while the electromagnetic properties are well reproduced. A similar behaviour was noticed in the neighbouring radon [58] and, up to some extent, mercury [69] isotopes. As presented in Figure 11 for ^{196}Po predictions of the GBH model are significantly better in this aspect, which may indicate importance of triaxial degrees of freedom [57, 67]. The reproduction of the experimental energy levels and, to a lesser extent, the quadrupole properties by the IBM model follows directly from the fit to the measured values of transition probabilities to fix the IBM Hamiltonian.

Interesting to note is the evolution of the $2_1^+ \rightarrow 0_{\rm gs}^+$ transition in the neutron-

deficient Po-Hg isotopes predicted by BMF model. The experimental transition probability between the ground state and the first excited 2_1^+ state in $^{198,196}Po_{114,112}$ is underestimated by the BMF model, and is in better agreement with the transition calculated for the 0_2^+ state. For the heavier masses of polonium isotopes, $A > 200$, the $2_1^+ \rightarrow 0_{gs}^+$ transition is well reproduced pointing out a proper description of underlying structure. As noted by Yao et al. [47], a change of structure for Po isotopes take place at $N = 114$ and an onset of oblate deformation is predicted already at $N = 112$. This is consistent with the results of the isotope shift measurements [16–18]. In the case of the mercury isotopes transition probabilities between the 2_1^+ and the ground state were correctly reproduced by the BMF model for $^{186}Hg_{106}$ and $^{188}Hg_{108}$. For more neutron-deficient $^{182,184}Hg_{102,104}$ the measured $2_1^+ \rightarrow 0_{gs}^+$ transitions are vastly overestimated while, again, better agreement with experiment was found for the $2_2^+ \rightarrow 0_2^+$ transition. This was interpreted as being related to a change of structure in the calculations between the ground and excited 0^+ states in neutron-deficient mercury isotopes [47] – going from an oblate-like ($N \geq 106$) to a prolate-like character (below $N < 106$). More generally, the GBH model overestimates quadrupole properties of the 2_1^+ state in all $^{182-188}$Hg, while these are well reproduced in all $^{196-202}$Po isotopes.

4. Summary and Outlook

Coulomb excitation of heavy exotic beams at REX-ISOLDE has spawned a large array of data on low-lying coexisting shapes. However, in all of the isotopes presented, the data are not complete. This technique has the potential to provide much richer information with higher beam energies utilising the larger multi-step excitation cross-section. HIE-ISOLDE [83] will bring about the required beam energies, but will also bring about its own problems. Fundamental to the interpretation of Coulomb-excitation data with exotic beams is the input of complementary spectroscopic data. In the case of mercury, it has been shown how lifetimes of excited-states provide an internal normalisation of the data, while γ-ray branching ratios constrain large sets of strongly correlated matrix elements [54]. Future multi-step Coulomb-excitation experiments at will provide interesting and important data, but without additional spectroscopic information, it may be difficult to draw conclusive results. Therefore, this new and exciting regime must be treated carefully and complementary experiments that provide the required constraints at higher excitation must to be carried out.

Clarification is required on the type of deformation of the intruding states in mercury. The two-band-mixing model studies of Refs. [34, 84] show that the yrast $B(E2)$ values cannot be reproduced if the two bands have opposite signs of deformation, yet a similar analysis of matrix elements suggests otherwise [53]. The quadrupole sum rules method can provide a nuclear model-independent answer given a large enough set of precisely measured matrix elements. Future experiments at HIE-ISOLDE intend to provide this data [85]. They will also benefit from the use of the electron spectrometer SPEDE [72] that will provide a direct way of detecting the $E0$ transitions, which are of

great importance for nuclei from the light lead region.

It was highlighted that in-source laser spectroscopy has extended the reach of deformation measurements of ground states. This has proved useful in giving the first indications of the behaviour of intruder states and level of mixing. Consistency between deformation parameters extracted from differences in mean-square-charge radii and the quadrupole sum rules method is shown, giving confidence to the systematic behaviour extracted from this data. With the new Collinear Resonant Ionisation Spectroscopy (CRIS) setup at ISOLDE [86], high-resolution spectroscopy can be performed on isotopes with more complex hyperfine structures, allowing extraction of magnetic-dipole and electric-quadrupole moments. The first measurements in this region have already proved successful with a study of francium isotopes [15, 87, 88].

Few-nucleon transfer reaction experiments are considered in the light lead mass region [89]. One idea is to use an isomerically pure beam of the odd-mass mercury, produced using laser ionisation of specific hyperfine components. Performing one-neutron transfer on such a beam will feed low-spin states in even-mass mercury and the relative cross sections could provide information on the intruder contribution and underlying structure of coexisting states. Further, two-proton transfer reactions might be a way to validate the common interpretation that proton-pair excitation across the $Z = 82$ proton shell closure is the driving mechanism behind shape coexistence in this mass region. These challenges may be fulfilled with the use of higher beam intensities, purities and energies, available up to 10 MeV/u at the final stage of HIE-ISOLDE project at CERN. Within this Coulomb-excitation experiments of odd-mass isotopes is also planned, e.g. ^{185}Hg, which aim to characterise the shape coexisting isomers present in mercury.

All of these efforts combined with new decay spectroscopy, mass measurements and laser spectroscopy profiting from HIE-ISOLDE, together with lifetime measurements, will result in precision characterisation of shape coexistence in atomic nuclei.

5. Acknowledgements

We would like to thank Nele Kesteloot for sharing her figures and data on Po, Freddy Flavigny for use of his Miniball drawings, Tuomas Grahn, Leszek Próchniak and Marcus Scheck for their comments on the manuscript and Janne Pakarinen for sharing his figures and data on Pb and his comments on the manuscript. This work was supported by GOA/2010/10 (BOF KU Leuven), by the IAP Belgian Science Policy (BriX network P6/23 and P7/12), and by the U.K. Science and Technology Facilities Council (STFC).

References

[1] Heyde K and Wood J L 2011 *Rev. Mod. Phys.* **83** 1467–1521

[2] Bijnens N *et al.* 1995 *Phys. Rev. Lett.* **75** 4571–4574

[3] Andreyev A N *et al.* 2000 *Nature* **405** 430–433

[4] Andreyev A N *et al.* 2002 *Phys. Rev. C* **66** 014313
[5] Van de Vel K *et al.* 2002 *Phys. Rev. C* **65** 064301
[6] Van de Vel K *et al.* 2003 *Phys. Rev. C* **68** 054311
[7] Kettunen H *et al.* 2005 *Eur. Phys. J. A* **25** 181–182
[8] Uusitalo J *et al.* 2005 *Phys. Rev. C* **71** 024306
[9] Andreyev A N *et al.* 2009 *Phys. Rev. C* **80** 054322
[10] Cocolios T E *et al.* 2010 *J. Phys. G Nucl. Part. Phys.* **37** 125103
[11] Elseviers J *et al.* 2011 *Phys. Rev. C* **84** 034307
[12] Pearson M R *et al.* 2000 *J. Phys. G Nucl. Part. Phys.* **26** 1829–1848
[13] De Witte H *et al.* 2007 *Phys. Rev. Lett.* **98** 112502
[14] Seliverstov M D *et al.* 2009 *Eur. Phys. J. A* **41** 315–321
[15] Flanagan K T *et al.* 2013 *Phys. Rev. Lett.* **111** 212501
[16] Cocolios T E *et al.* 2011 *Phys. Rev. Lett.* **106** 052503
[17] Seliverstov M *et al.* 2013 *Phys. Lett. B* **719** 362–366
[18] Seliverstov M D *et al.* 2014 *Phys. Rev. C* **89** 034323
[19] The Windmill Collaboration *et al.* 2014 *β-delayed fission and in-source laser spectroscopy in the lead region* CERN-INTC **013** SR-029
[20] Gaffney L P *et al.* 2014 *In-source laser spectroscopy of mercury isotopes* CERN-INTC **060** P-424
[21] Garg U *et al.* 1986 *Phys. Lett. B* **180** 319–323
[22] Dracoulis G D *et al.* 1986 *J. Phys. G Nucl. Phys.* **12** L97–L103
[23] Walpe J, Garg U, Naguleswaran S and Ren Q 1995 *Acta Phys. Pol. B* **26** 279
[24] Joshi P *et al.* 2002 *Phys. Rev. C* **66** 044306
[25] Dewald A *et al.* 2003 *Phys. Rev. C* **68** 034314
[26] Joshi P *et al.* 2004 *Phys. Rev. C* **69** 044304
[27] Chamoli S K *et al.* 2005 *Phys. Rev. C* **71** 054324
[28] Grahn T *et al.* 2006 *Phys. Rev. Lett.* **97** 062501
[29] Chamoli S K *et al.* 2007 *Phys. Rev. C* **75** 054323
[30] Grahn T *et al.* 2009 *Phys. Rev. C* **80** 014324
[31] Scheck M *et al.* 2010 *Phys. Rev. C* **81** 014310
[32] Gladnishki K *et al.* 2012 *Nucl. Phys. A* **877** 19–34
[33] Walpe J C *et al.* 2012 *Phys. Rev. C* **85** 057302
[34] Gaffney L P *et al.* 2014 *Phys. Rev. C* **89** 024307
[35] Muikku M *et al.* 1998 *Phys. Rev. C* **58** R3033–R3036
[36] Taylor R *et al.* 1999 *Phys. Rev. C* **59** 673–681
[37] Jenkins D *et al.* 2000 *Phys. Rev. C* **62** 021302
[38] Julin R, Helariutta K and Muikku M 2001 *J. Phys. G Nucl. Part. Phys.* **27** R109–R139
[39] Dracoulis G D *et al.* 2003 *Phys. Rev. C* **67** 051301
[40] Reviol W *et al.* 2003 *Phys. Rev. C* **68** 054317
[41] Pakarinen J *et al.* 2005 *Phys. Rev. C* **72** 011304

[42] Rahkila P *et al.* 2010 *Phys. Rev. C* **82** 011303

[43] Scheck M *et al.* 2011 *Phys. Rev. C* **83** 037303

[44] Julin R, Grahn T, Rakhila P and Pakarinen J *this issue*

[45] Bonn J, Huber G, Kluge H J, Kugler L and Otten E 1972 *Phys. Lett. B* **38** 308–311

[46] Ulm G *et al.* 1986 *Zeitschrift für Phys. A At. Nucl.* **325** 247–259

[47] Yao J M, Bender M and Heenen P H 2013 *Phys. Rev. C* **87** 034322

[48] García-Ramos J E and Heyde K 2014 *Phys. Rev. C* **89** 014306

[49] Kumar K 1972 *Phys. Rev. Lett.* **28** 249–253

[50] Cline D 1986 *Annu. Rev. Nucl. Part. Sci.* **36** 683–716

[51] Jenkins D G 2014 *Nat. Phys.* **10** 909–913

[52] Görgen A 2010 *J. Phys. G Nucl. Part. Phys.* **37** 103101

[53] Bree N *et al.* 2014 *Phys. Rev. Lett.* **112** 162701

[54] Bree N 2014 *Shape coexistence in the neutron-deficient mercury isotopes studied through Coulomb excitation* PhD KU Leuven

[55] Clément E *et al.* 2007 *Phys. Rev. C* **75** 054313

[56] Pakarinen J *et al.* 2015 *J. Phys. Soc. Japan Conf. Proc.* **6** 020011

[57] Kesteloot N *et al.* 2015 *Phys. Rev. C (accepted)*

[58] Gaffney L P *et al.* 2015 *Phys. Rev. C* **91** 064313

[59] Grahn T *et al.* 2013 *EPJ Web Conf.* **63** 01009

[60] Marsh B *et al.* 2013 *Nucl. Instrum. Meth. B* **317** 550–556

[61] Penescu L, Catherall R, Lettry J and Stora T 2010 *Rev. Sci. Instrum.* **81** 02A906

[62] Ames F *et al.* 2005 *Nucl. Instrum. Meth. A* **538** 17–32

[63] Wenander F 2010 *J. Instrum.* **5** C10004

[64] Voulot D *et al.* 2008 *Nucl. Instrum. Meth. B* **266** 4103–4107 proceedings of the XVth International Conference on Electromagnetic Isotope Separators and Techniques Related to their Applications

[65] Warr N *et al.* 2013 *Eur. Phys. J. A* **49** 40

[66] Zielińska M *et al.* 2015 *arXiv preprint* arXiv:1506.04633

[67] Kesteloot N 2015 *Deformation and mixing of co-existing shapes in the neutron-deficient polonium isotopes* PhD KU Leuven

[68] Bree N *et al.* 2015 *Nucl. Instrum. Meth. B* **360** 97–102

[69] Wrzosek-Lipska K *et al.* 2015 *Phys. Rev. C (in preparation)*

[70] Czosnyka T, Cline D and Wu C Y 1983 *Bull. Am. Phys. Soc.* **28** 745

[71] Cline D *et al.* 2012 *Gosia User Manual for Simulation and Analysis of Coulomb Excitation Experiments* (Rochester, NY, US: `http://www.pas.rochester.edu/$\sim$cline/Gosia/Gosia_Manual_20120510.pdf`)

[72] Papadakis P *et al.* 2015 The SPEDE Spectrometer: Combined In-Beam γ-ray and Conversion Electron Spectroscopy with Radioactive Ion Beams *Proc. Conf. Adv. Radioact. Isot. Sci.* (Journal of the Physical Society of Japan) ISBN 4-89027-110-4

[73] Pakarinen J *et al.* 2013 *Probing intruder configurations in* ^{186,188}*Pb using Coulomb excitation* CERN-INTC **004** P-370

[74] Srebrny J and Cline D 2011 *Int. J. Mod. Phys. E* **20** 422–430

[75] Wrzosek-Lipska K *et al.* 2012 *Phys. Rev. C* **86** 064305

[76] Próchniak L and Rohoziski S G 2009 *J. Phys. G Nucl. Part. Phys.* **36** 123101

[77] Otten E W 1989 *Treatise Heavy-Ion Sci.* **8** 517–638

[78] Borchers W *et al.* 1987 *Hyperfine Interact.* **34** 25–29

[79] Georg U *et al.* 1995 Laser spectroscopy of ^{200}Rn and ^{201}Rn using alpha detection *Int. Conf. Exot. Nucl. At. Masses ENAM '95* ed De Saint-Simon O and Sorlin O (Arles, France) pp 133–134 ISBN 2863321862

[80] Mariscotti M A J, Scharff-Goldhaber G and Buck B 1969 *Phys. Rev.* **178** 1864–1886

[81] Lane G J *et al.* 1995 *Nucl. Phys. A* **589** 129–159

[82] Heenen P H and Bender M *this issue*

[83] Lindroos M, Butler P, Huyse M and Riisager K 2008 *Nucl. Instrum. Meth. B* **266** 4687–4691

[84] Guttormsen M 1981 *Phys. Lett. B* **105** 99–102

[85] Wrzosek-Lipska K *et al.* 2012 *Coulomb excitation of* $^{182-184}$*Hg: Shape coexistence in the neutron-deficient lead region* CERN-INTC **063** P-364

[86] Cocolios T E *et al.* 2013 *Nucl. Instrum. Meth. B* **317** 565–569

[87] Lynch K M *et al.* 2014 *Phys. Rev. X* **4** 011055

[88] Budinčević I *et al.* 2014 *Phys. Rev. C* **90** 014317

[89] Van Duppen P *et al.* 2010 *Shape coexistence in the neutron-deficient region around* $Z = 82$ *studied via Coulomb excitation and few-nucleon transfer reactions* CERN-INTC **044** I-110